2. Quasi-Poloidally-Symmetric Configurations

This chapter describes the characteristics of quasi-poloidally-symmetric magnetic configurations and relevant physics issues.

An important property of the QPS reference configuration is the approximate poloidal symmetry of the |B| spectrum in the plasma interior (away from the edge of the plasma). This feature identifies QPS as having unique properties not shared by other quasi-symmetric configurations such as NCSX (a quasi-axisymmetric device) and HSX (a quasi-helically symmetric stellarator). One such property is the presence of a finite number of trapped particles all the way to the magnetic axis. This implies that the bootstrap current can be non-zero on axis (provided $dp/d\psi \neq 0$), thus obviating the need for a seed current to generate finite rotational transform on axis. Another is the small poloidal viscosity compared to the toroidal viscosity, which should result in distinctly different flow control strategy – and hence control of the radial electric field – in QPS compared to quasi-axisymmetric (or helical) configurations. Also, the internally generated transform due to the bootstrap current is small compared to the external transform in QPS, and makes the equilibrium configuration somewhat invariant as β is varied.

2.1. Consequences of Poloidal Symmetry

The transport properties of QPS are direct consequences of the approximate poloidal symmetry of the |B| spectrum. The dominant spectral coefficients of |B| in Boozer coordinates for the reference QPS configuration are shown in Figure 2.1. In this coordinate system the magnitude of the magnetic field can be expressed in a Fourier spectrum as

$$|B| = \Sigma\, B_{mn}(\psi) \cos(m\theta - n\phi)$$

where θ and ϕ are poloidal and toroidal angle variables and ψ is the toroidal flux. It can be seen that for interior magnetic surfaces away from the plasma boundary $\rho \equiv \psi^{1/2} = 1$, the spectrum is dominated by the $m = 0$, $n = 1$ (in field period units) "linked-mirror" component, i.e., |B| exhibits approximate poloidal symmetry, $\partial|B|/\partial\theta \approx 0$. Near the edge, there is a $1/R$ component ($m = 1$, $n = 0$), of comparable magnitude to the $m = 0$, $n = 1$ component, which violates the quasi-poloidal symmetry. In addition there is a smaller helical component near the edge which decays away inside the plasma This structure is similar to the large-A_p W 7-X spectra associated with omnigenity-optimized transport. However, the cancellation of the bootstrap current in W 7-X which occurs over the entire plasma cross-section is not present in the QPS design, as discussed below. The effective magnetic aspect ratio based on the $m = 1$, $n = 0$ component of |B| (the $1/R$ field) is $A_{p,magnetic} \sim 5$, which is $2A_p$ (here, A_p is the geometric aspect ratio R/a). This indicates a reduction in the grad |B| drift associated with this component of |B|. There is a substantial magnetic ripple associated with the mirror field component, corresponding to a mirror ratio (B_{max}/B_{min}) ~2 for the QPS configurations considered here.

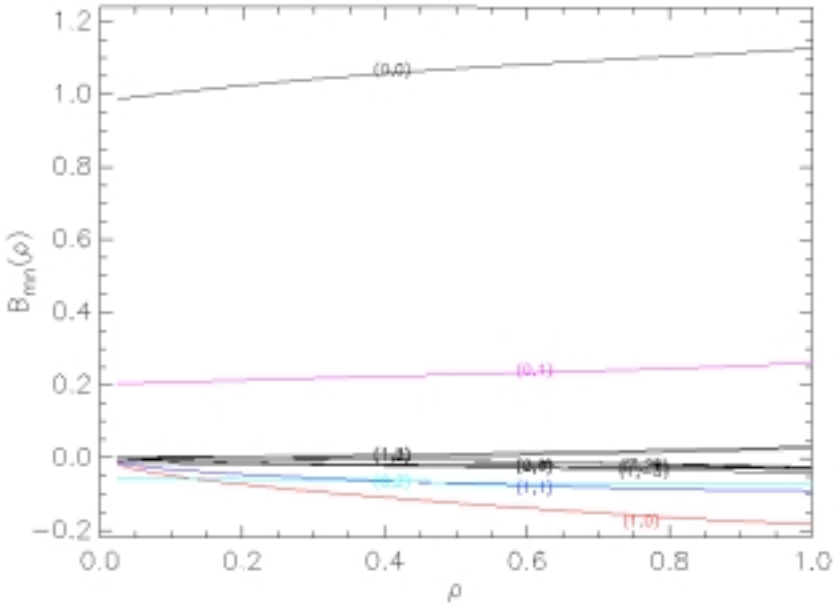

Figure 2.1. |B| spectrum for the reference QPS configuration.

In the limit of *exact* poloidal symmetry, the canonical angular momentum $p_{\theta_} = mv_{\theta_} + eA_{\theta_}$ is conserved. Particle orbit excursions would be limited to the gyroradius in the *toroidal* field, which is usually much smaller than the *poloidal* gyroradius (banana width) characteristic of orbit widths in quasi-axisymmetric devices (e.g., NCSX or tokamaks). This reduction in orbit size implies a concomitant reduction in the bootstrap current compared to tokamaks. Thus QPS tends to operate either with a significantly smaller bootstrap current than in axisymmetric devices (for the same ι, or $1/q$, the potential reduction is ~ι/N) and/or at lower ι (higher q). Note that the implied smaller poloidal flux in QPS does not necessarily lead to increased neoclassical losses because the limiting orbit size is the toroidal gyroradius, which remains quite small.

Poloidally symmetric plasmas are, in Boozer coordinates at least, similar to "linked-mirrors" without end losses (which are eliminated due to the toroidal geometry). However, because of the finite rotational transform in QPS, the magnetic field lines are generally ergodically distributed over the magnetic surface (except at rational surfaces), making the transport and stability properties of QPS plasmas more closely related to those of other quasi-symmetric stellarators rather than to mirror-like (EBT) devices.

The effect of quasi-poloidal symmetry on neoclassical transport can be understood from Figure 2.2, which shows the |B| contours (solid curves) and magnetic field lines (red straight dashed lines) for QPS at the magnetic flux surface $S = 0.7$. Here $S \sim (r/a)^2$ where r is the average radius of a flux surface. Since the radial motion of particles is given by the B x grad |B| drift, the approximate alignment of B and grad |B| directions implies a suppression of these drift effects *away* from the magnetic surfaces. This has the potential

to significantly reduce both the neoclassical energy and particle losses as well as the self-consistent bootstrap current.

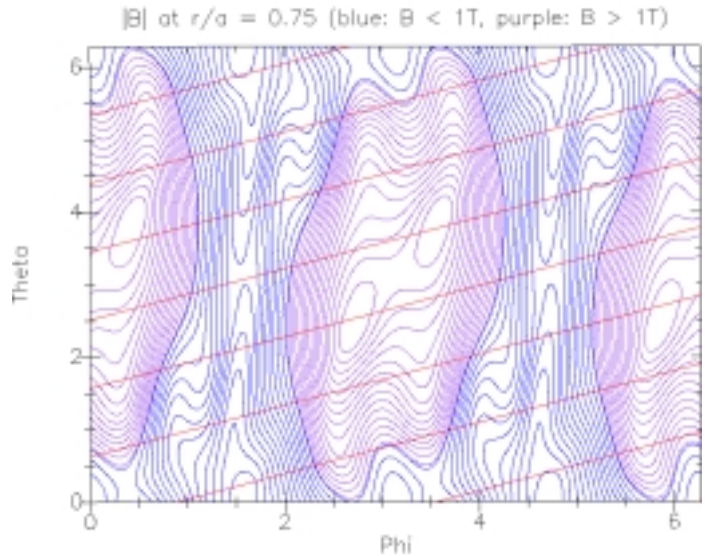

Figure 2.2. Contours of |B| on the r/a = 0.75 surface for the reference configuration.

QPS exhibits departures from quasi-symmetry which typically decrease rapidly away from the edge of the plasma (see Figure 2.1). Such a departure from exact quasi-poloidal symmetry in QPS is desirable to drive a small, but finite, self-consistent bootstrap current. Typically, the bootstrap current varies from ~30% (at the center) to ~ 50% (at the edge) of the value that would occur in a tokamak with similar ι profile, as shown in Figure 2.3. The presence of internal bootstrap current at finite β values relieves some of the burden on the coils for producing rotational transform. This reduces the helical excursion of the coils, producing a more compact configuration, and thereby facilitates the engineering of coils at low aspect ratios. In addition, small bootstrap currents can increase ballooning stability limits by reducing unfavorable helical curvature (although opposite, destabilizing effects have also been observed in other configurations), without introducing vertical or kink modes in the plasma. The calculations for the QPS reference configuration have been performed to make the bootstrap current profile and magnitude approximately self-consistent with the ι and pressure profiles. A low collision-frequency analytic expression for the bootstrap current is used as an approximation for j_{bs} in QPS. Finite ν^* corrections, as well as the effect of the radial electric field at low collisionalities, have been calculated using both Monte Carlo and DKES codes and are shown in Figure 2.4. Both effects tend to reduce the magnitude of the bootstrap Onsager coefficient L_{13} for anticipated operating regimes of the experiment. However, since the fraction of rotational transform arising in QPS from the bootstrap current at or near the highest stable $\langle\beta\rangle$ < 2% is typically small (ι_{bs}/ι_{total} ~ 20%, see Figure 2.5), the variation with β and ν^* of this internal current should have a minimal impact on the experiment. The dependence of the bootstrap current at low aspect ratio on

both the temperature and electric potential remains an interesting experimental feature to be measured.

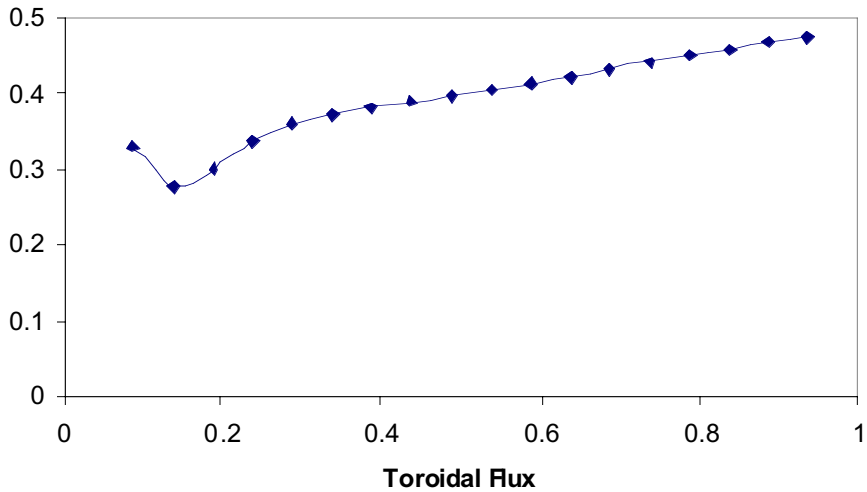

Figure 2.3. Ratio of the bootstrap current on the reference design to the bootstrap current in an equivalent tokamak.

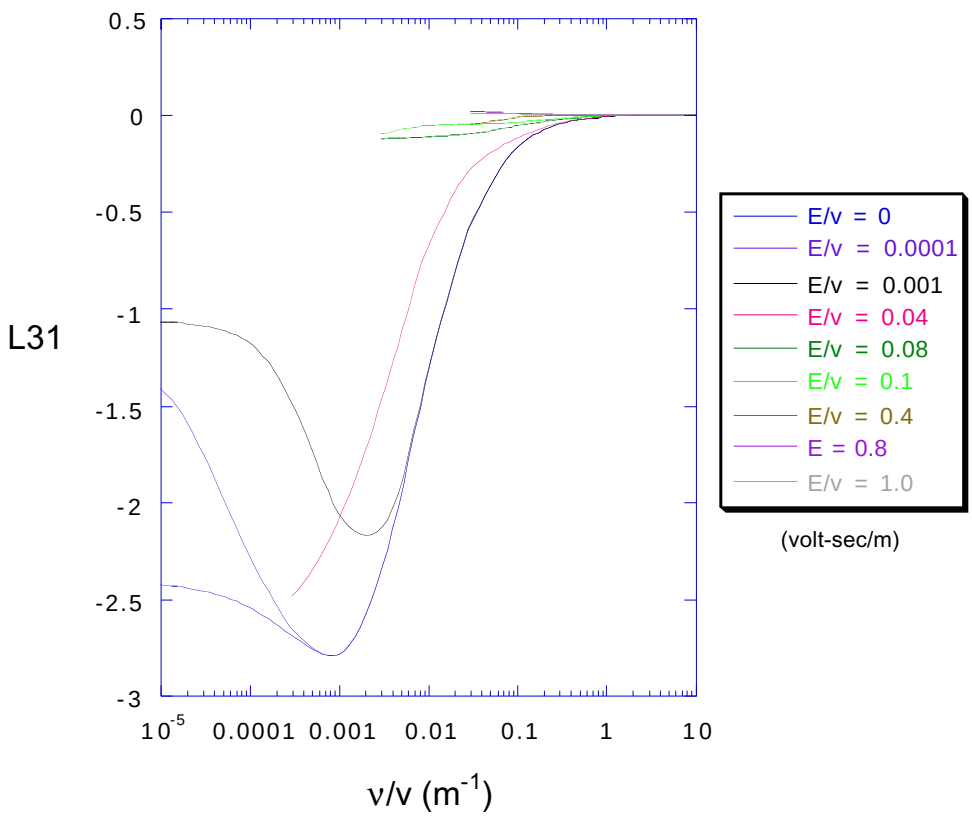

Figure 2.4. Effect of finite-ν* corrections and the radial electric field at low collisionalities on the bootstrap current.

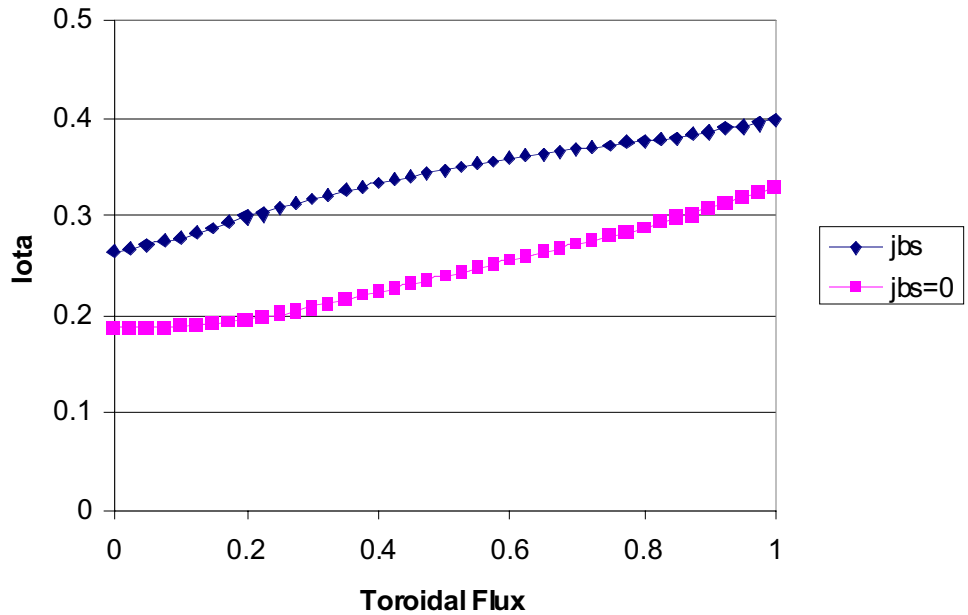

Figure 2.5. Effect of the bootstrap current on the rotational transform profile for the reference configuration at $\langle\beta\rangle = 2\%$.

Note from Figure 2.5 that the bootstrap current flows along the magnetic field so that the rotational transform it produces *adds* to the existing external transform arising from coils. This feature, together with the positive shear throughout the plasma (ι increasing radially everywhere in the plasma), makes the QPS configuration stable to neoclassical tearing modes, i.e. $j_{bs}*\iota'/\iota > 0$. This is another desirable effect of the small self-consistent bootstrap current in QPS, which is anticipated to reduce the size of magnetic islands as β increases.

The degree of quasi-poloidal symmetry for the reference QPS GB4 configuration, and for improvements to it from the GB5 series, decreases on a flux surface in going from the plasma interior to the edge, as indicated in Figure 2.6 which shows the ratio of magnetic energy in non-quasi-poloidal modes to that in quasi-poloidal modes vs. $(\psi/\psi_{edge})^{1/2} \approx r/a$. Near the plasma edge these configurations have a more quasi-omnigenous character.

Departures from poloidal symmetry can increase neoclassical transport in QPS in much the same way that ripple losses deteriorate confinement in tokamaks in the low collision frequency regime. This potentially deleterious effect for QPS has been estimated using Monte Carlo techniques for both thermal and energetic (RF-heated) particles. In practice, this evaluation is performed *after* the optimization process is completed, due to the time-consuming nature of Monte Carlo calculations as well as the statistical noise associated with finite particle populations which makes it difficult to evaluate numerically stable targets for the transport optimization, as discussed in detail in Chapter 3. Near the edge of QPS, where departures from poloidal symmetry are largest, omnigeneity can reduce the $1/\nu$

transport by producing partial alignment of drift surfaces with magnetic flux surfaces. This effect has been used to reduce the edge transport in QPS.

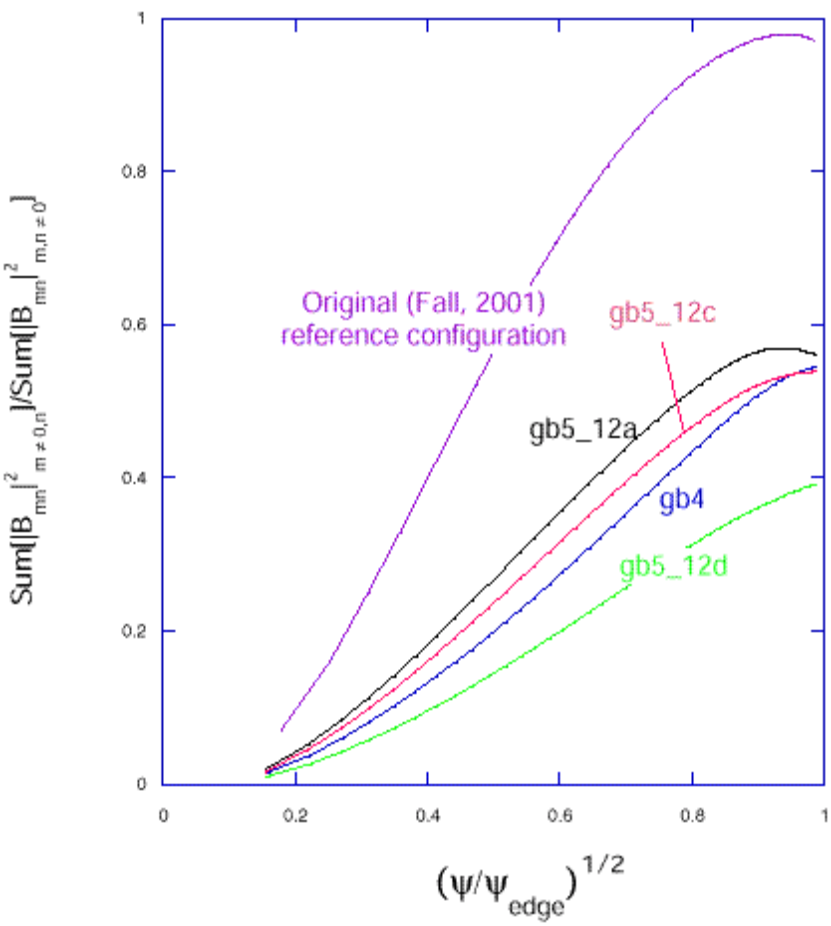

Figure 2.6. Degree of quasi-poloidal symmetry versus minor radius for several candidate QPS configurations.

The control of the radial profile of the electric field is important for suppressing turbulence and hence accessing enhanced confinement regimes in stellarators and tokamaks. In quasi-axisymmetric devices, the plasma flow is viscously damped in the poloidal direction due to magnetic pumping in the $1/R$ field and the radial field can be experimentally affected by the magnitude of the toroidal flow. The quasi-poloidal symmetry in the interior of QPS causes a damping process in the orthogonal (toroidal) direction, since the dominant magnetic pumping occurs due to the toroidal ripple wells. This leads to much smaller toroidal flows than in a quasi-axisymmetric system. Thus, the poloidal flow will be the control knob available for adjusting the level of turbulence in QPS configurations.

2.2. Quasi Poloidal Configurations at High Beta

Whereas the reference QPS configuration has relatively modest β limits (set by high-n ballooning modes), it is related to a class of QPS-optimized stellarators which possess a much higher β limit (⟨β⟩ > 10%) and a moderate bootstrap current. Figure 2.7 shows the outer flux surfaces of an N = 2, R/a = 2.6, ⟨β⟩ = 10%, quasi-poloidally-symmetric (QPS) configuration with contours of |B| indicated in color. Figure 2.8 shows a higher-β (⟨β⟩ = 15%), N = 3, R/a = 3.7 QPS configuration.

This class of QPS configurations exhibits properties of a tokamak-stellarator hybrid with a |B|-spectrum possessing quasi-poloidal symmetry similar to QPS, as shown in Figure 2.9.

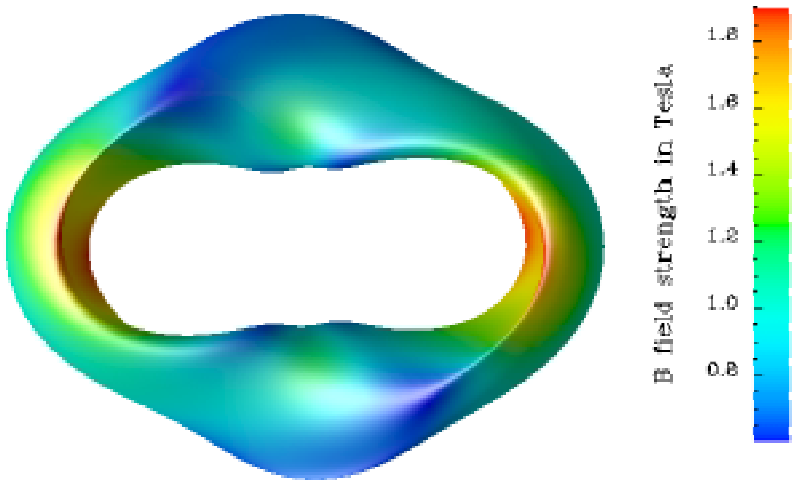

Figure 2.7. |B| values and shape of the LCFS for a QPS configuration at ⟨β⟩ = 10%.

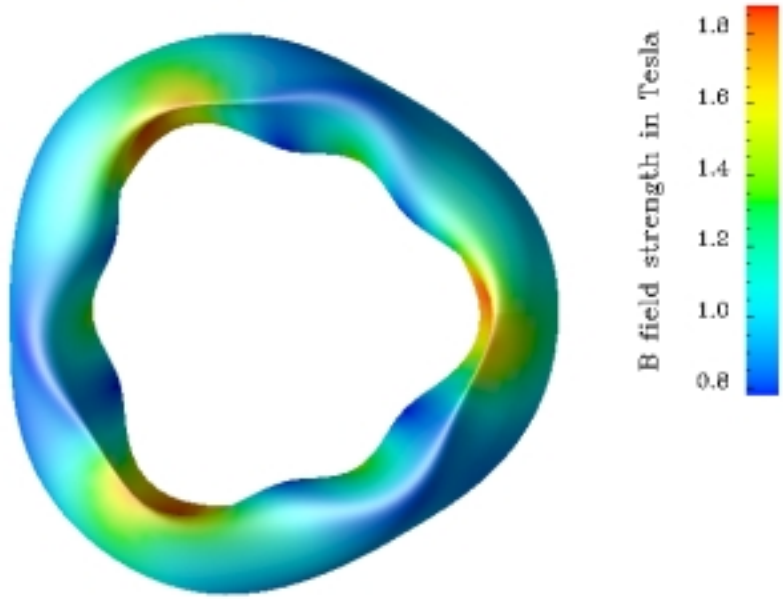

Figure 2.8. |B| values and shape of the LCFS for a QPS configuration at ⟨β⟩ = 15%.

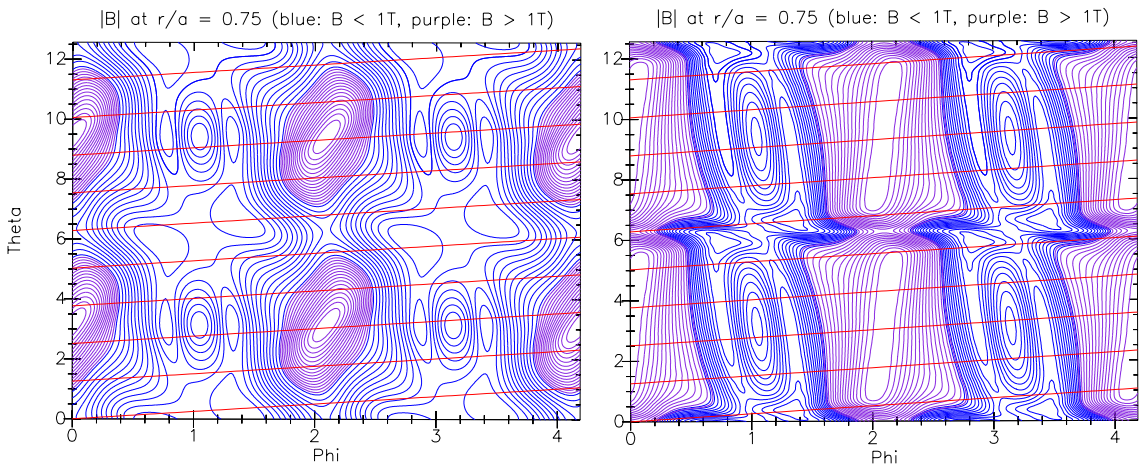

Figure 2.9. |B| values vs. toroidal angle (Theta) and poloidal angle (Phi) at r/a = 0.75 for the N = 3 QPS configuration at $\langle\beta\rangle$ = 0 (left) and $\langle\beta\rangle$ = 23% (right).

Unlike the other plots of $|B|(\theta, \phi)$ on a constant r/a surface in this document, the θ coordinate is plotted for two poloidal turns (4π) rather than once around the torus poloidally. The degree of quasi-poloidal symmetry increases with β, as shown in Figure 2.10 for the N = 3, R/a = 3.7 QPS configuration. The $m \neq 0$ terms decrease with increasing β and the B_{00} term, the average value of |B| on a flux surface, decreases in the center as β increases.

These configurations have a high shear, tokamak-like transform profile (i.e., ι *decreases* radially) and have transport properties for both thermal and energetic particles which improve with β. The non-axisymmetric components of the |B| spectrum result in a reduced bootstrap current compared to a tokamak with the same ι and p profiles. These configurations achieve bootstrap alignment (i.e., the bootstrap current supplies all the required equilibrium current) at substantially reduced values of field-aligned (parallel) current, 1/5-1/3 that of a similar tokamak. This finite, but lower, current results in MHD stability at higher values of β: $\langle\beta\rangle$ > 20% for Mercier and ballooning stability and $\langle\beta\rangle$ ~ 11% for vertical and kink stability.

In contrast with the concept-exploration QPS configurations, these hybrid QPS configurations have only a small external rotational transform arising from coils (typically, ι_{coils} ~ 0.05-0.10, where ι_{coils} is the rotational transform due to external coils). Thus the rotational transform profile is related to the internal plasma current profile much like in a tokamak. For the configuration shown in Figure 2.8, ι varies monotonically between 0.4 on axis to 0.1 at the edge, with approximately half of the small edge transform arising from currents in external coils. Note that this profile completely avoids the ι = 1/2 resonance (internal disruptions are suppressed) and other low-order resonances.

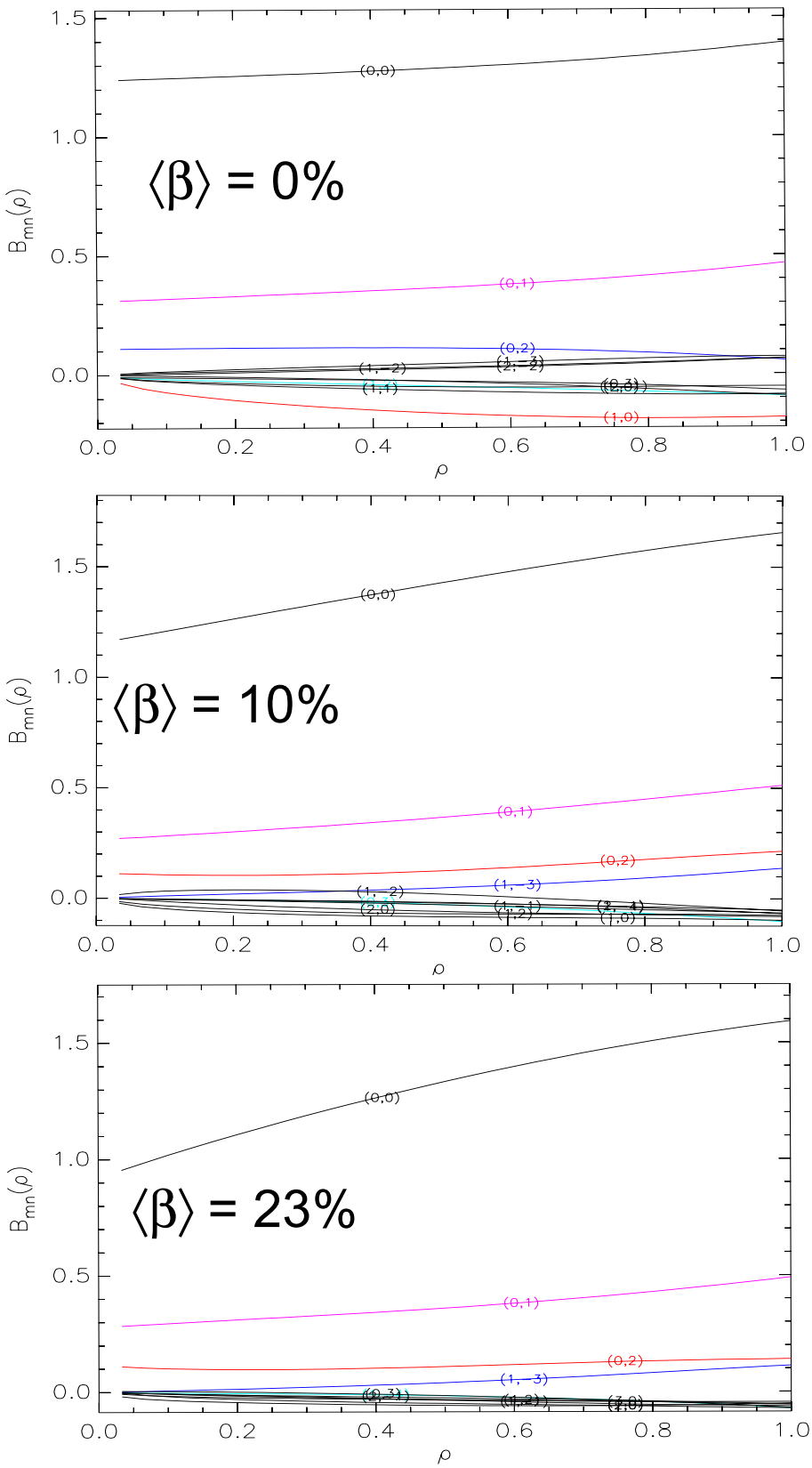

Figure 2.10. |B| spectrum for the N = 3 QPS configuration in Figure 2.8 as ⟨β⟩ increases.

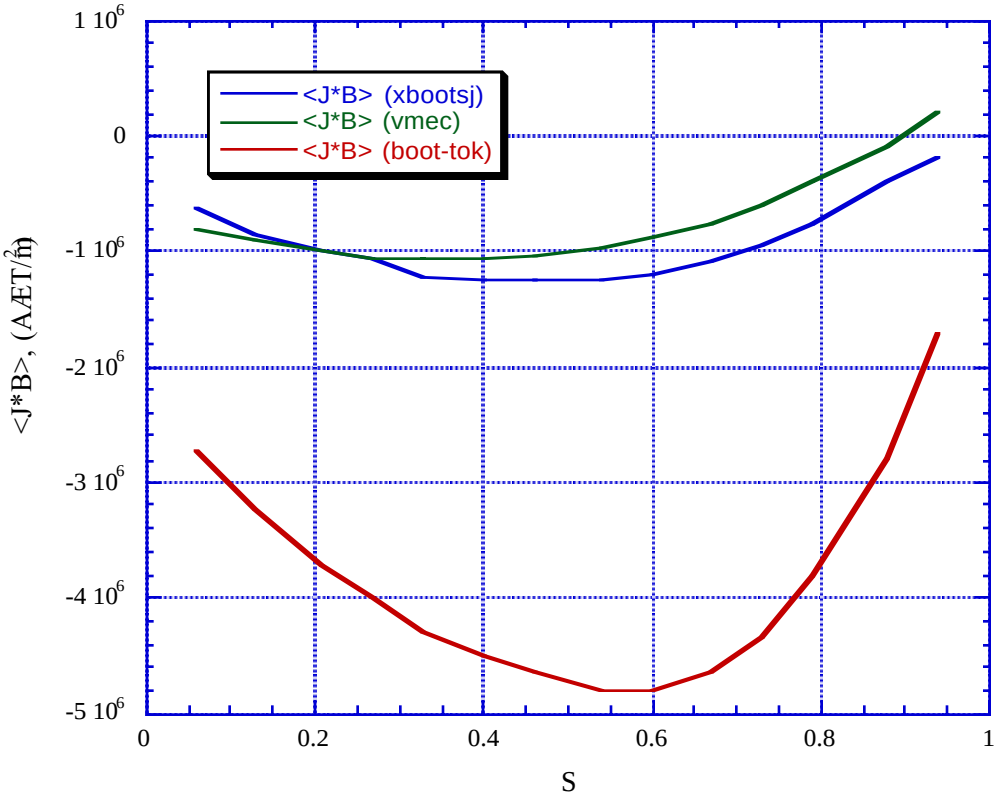

Figure 2.11. Bootstrap current and equilibrium current (VMEC) for QPS configuration in Figure 2.8.

The main effect of the external coils in these configurations is to substantially reduce (but not completely suppress) the self-consistent bootstrap current arising at finite β. Configurations were optimized for alignment of the equilibrium and bootstrap currents. Figure 2.11 shows the profiles of the field-aligned (parallel) current, the predicted bootstrap current, and the predicted bootstrap current in an equivalent tokamak (a torus with the same axisymmetric boundary shape and rotational transform) as a function of the flux variable *S* for the configuration shown in Figure 2.8. The reduction in bootstrap current in QPS (~1/5 - 1/3 that of the equivalent tokamak) is due to the approximate quasi-poloidal symmetry of the |B| spectrum (similar to toroidally-linked mirrors). To achieve such a low equilibrium current in a tokamak would require an oppositely driven current to cancel the bootstrap current. Self-consistent bootstrap current profiles have been obtained in the range 2% < ⟨β⟩ < 23% which require little seed current (except in a very small volume near the magnetic axis: to achieve the optimized rotational transform profile. Also, the L13 Onsager coefficient (relating the bootstrap current to the pressure gradient) also decreases with β in such a way that L13 ~ j_{bs} is nearly independent of β for ⟨β⟩ > 7%. This leads to a nearly β-independent bootstrap current in this range and gives a degree of configurational invariance similar to

that achieved in W 7-X with zero bootstrap current. Figure 2.12 shows the bootstrap transport coefficient as a function of collisionality for several values of ⟨β⟩.

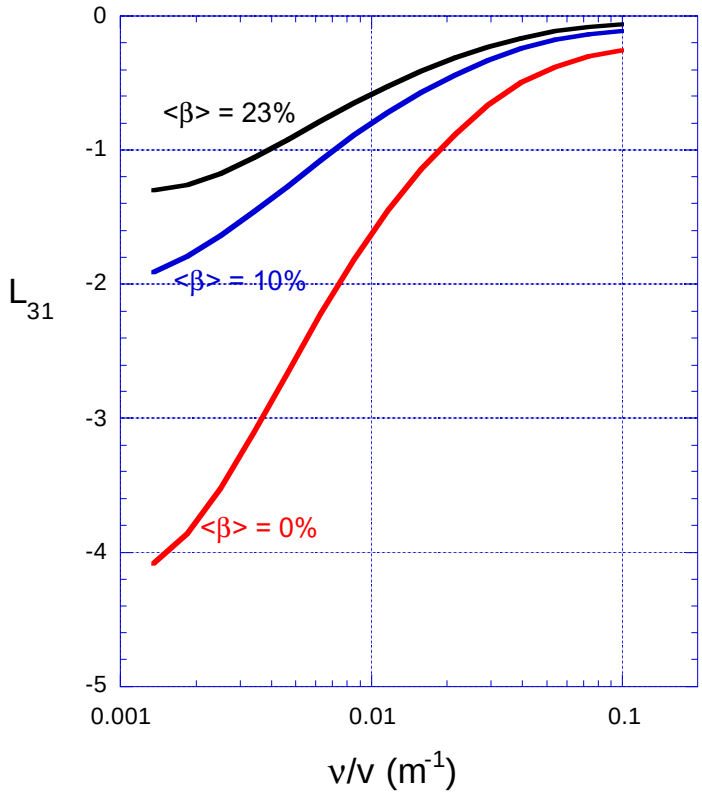

Figure 2.12. Approximate constancy of the bootstrap current with β.

The presence of somewhat larger bootstrap currents (due primarily to the larger stable β) distinguishes these configurations from the very low bootstrap current QPS devices previously discussed and results in reductions of both the helical curvature and the connection length in QPS. This gives rise to the higher ballooning stability β limits observed. The ballooning stability β-limit for these configurations was found to exceed ⟨β⟩ > 23%. By optimizing the plasma shape (outer flux surface), rotational transform profile, and pressure profile for a target β, ballooning stable configurations with good bootstrap alignment in the range 2% < ⟨β⟩ < 23% were obtained. For the three-field period, high-β QPS configurations, decreasing β while holding the shape and rotational transform profile fixed resulted in ballooning unstable configurations (unless β was lowered substantially). This is an indication that these plasmas are in the second-stable ballooning regime, as shown in Figure 2.13. In addition to the good ballooning stability, these configurations have good Mercier stability properties with a magnetic well over the entire cross section producing the dominant stabilization effect. The configuration in Figure 2.8 is Mercier stable except at the ι = 1/5 resonance, which occurs deep inside the plasma. The stabilizing magnetic well increases with increasing β, as indicated by the shift in the magnetic axis in the flux surfaces at ⟨β⟩ = 23% in Figure 2.14.

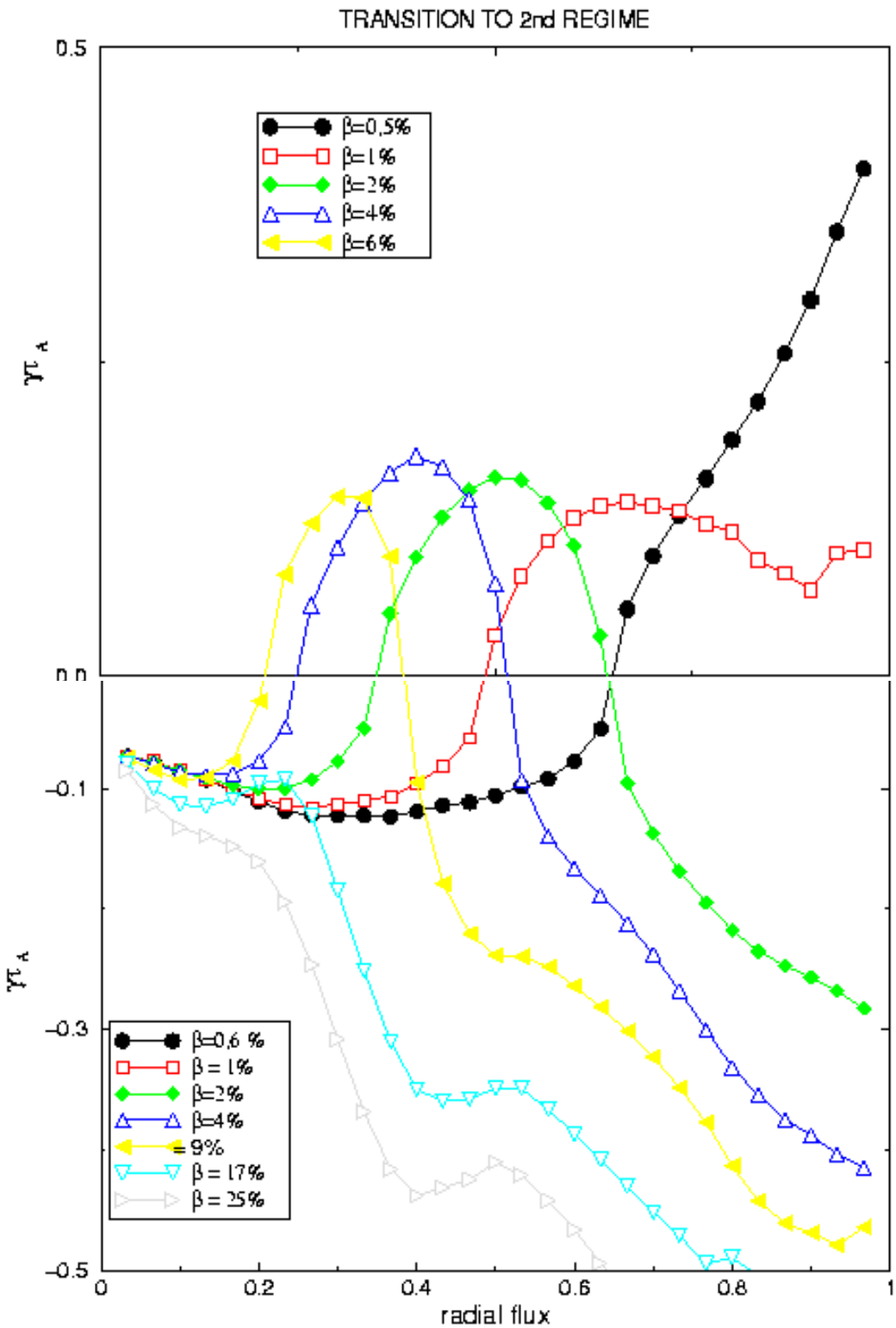

Figure 2.13. Transition to second ballooning stability in QPS occurs first near the plasma edge.

The presence of finite plasma current in QPS configurations makes them susceptible to vertical and kink modes. In spite of the finite plasma current and high β, the configuration shown in Figure 2.8 is stable to vertical modes and only weakly unstable to an external kink mode for $\langle\beta\rangle$ = 15%. Keeping the same shape but scaling $\langle\beta\rangle$ down to ~11% (but without modifying the rotational transform) leads to stabilization of the kink mode. At this β, the Troyon factor ($\beta_N = \beta(\%)[a(m)B(T)/I(MA)]$) is β_N = 19. This is a significantly larger value of β (for kink-stability) than in the equivalent tokamak with no wall stabilization. In combination with the lower current compared with a tokamak, this feature gives rise to the large Troyon factor. Stabilization of these low-n macroscopic modes should also be possible through either current profile tailoring (adjusting the bootstrap current near the plasma edge) or dynamic feedback provided by suitable external coils as is done for shaped tokamaks (although this is less desirable than passive stabilization afforded by the combination of small external rotational transform and reduced internal current).

The quasi-poloidal symmetry of these high-β configurations also results in acceptable neoclassical confinement times for both thermal and energetic particles. Ion and electron neoclassical confinement times were estimated using a Monte Carlo calculation. For $\langle|B|\rangle$ = 1 T and in the low collision frequency regime, we find τ_{Eneo}/τ_{ISS95} = 3-5 for expected values of the radial electric field and with a confinement enhancement factor H-ISS95 = 1. The electron neoclassical transport rate is a factor of 3-5 smaller and is hence negligible. Under these conditions, anomalous processes should dominate the thermal transport. The transport of the high-β configurations has also been tested and enhanced using a drift kinetic equation solver in the optimization code. Factors of 2 improvement in τ_{Eneo} were obtained by minimizing the local transport coefficients at several surfaces without sacrificing ballooning and kink stability. Furthermore, as β increases, the drift and flux surfaces achieve better alignment (attaining a nearly "omnigeneous" state). This not only improves thermal transport, but alpha particle confinement is also calculated to improve with increasing β. For the highest β's we have attained in these configurations (in the range of 15-20%), alpha-particle energy losses are around 10% for a reactor-scale device (B = 5 T, R = 10 m).

The small external transform and low number of field periods in QPS result in relatively simpler modular coils compared with conventional, lower current, compact QPS stellarators. Preliminary modular coils for an N = 3, R/a = 3.7 compact stellarator have been obtained with adequate distances between the plasma and the coils, as well as between adjacent coils needed for plasma heating and diagnostic access. Values of the ratio of coil separation to minor radius are found which imply favorable scaling to compact-reactor sizes.

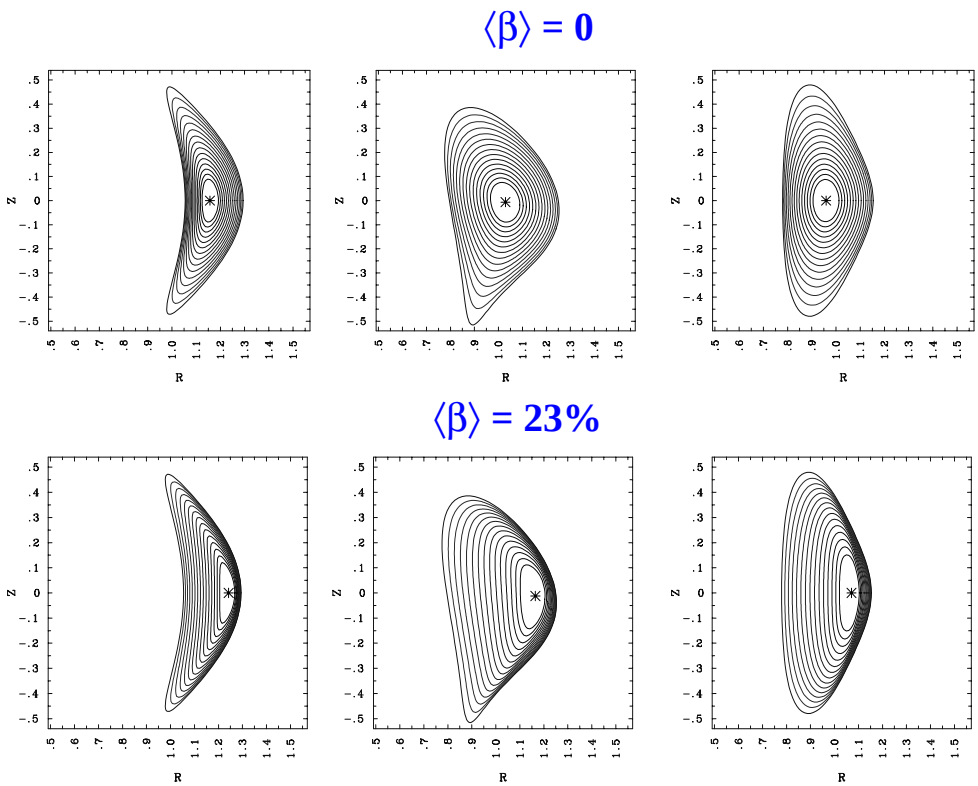

Figure 2.14. Magnetic well increases with increasing ⟨β⟩ for the N = 3 QPS configuration.

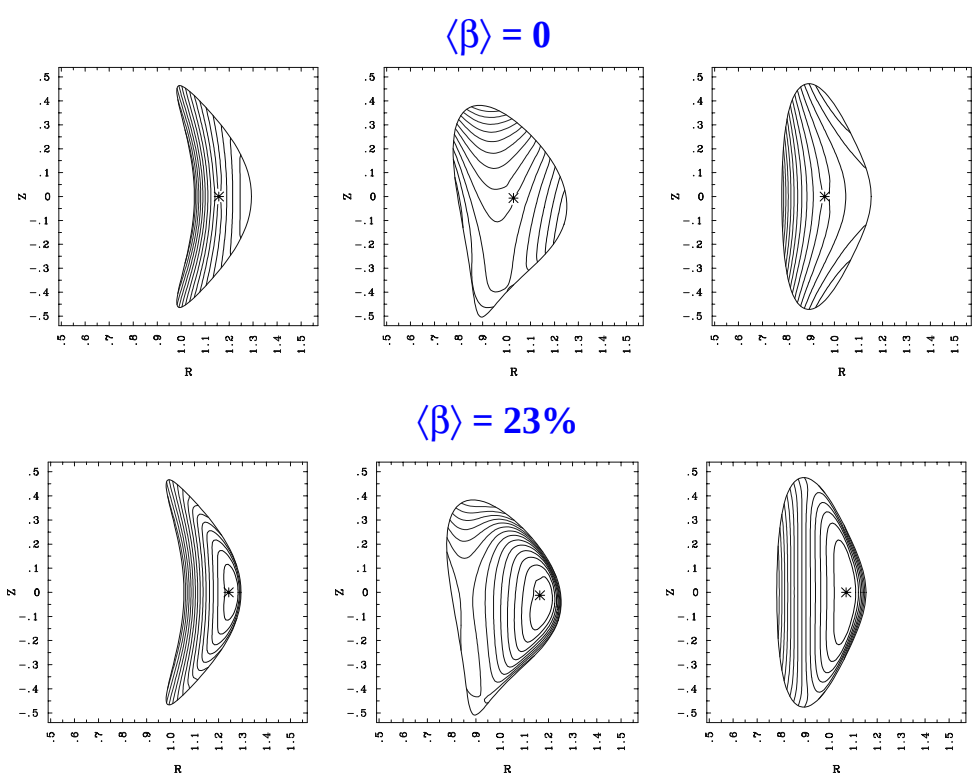

Figure 2.15. |B| contours close with increasing ⟨β⟩ for the N = 3 QPS configuration.